Optical Engineering

SPIEDigitalLibrary.org/oe

Real-time monitoring of phase maps of digital shearography

Lianqing Zhu
Yonghong Wang
Nan Xu
Sijin Wu
Mingli Dong
Lianxiang Yang

SPIE

Real-time monitoring of phase maps of digital shearography

Lianqing Zhu
Beijing Information Science and Technology University
School of Instrument Science and Opto-Electronic Engineering
12 E. Xiaoyin Rd., Qinghe of Haidan District
Beijing 100192, China

Yonghong Wang
Hefei University of Technology
School of Instrument Science and Opto-Electronic Engineering
59 Tunxi Rd., Hefei 230009,China

Nan Xu
Oakland University
Department of Mechanical Engineering
Optical Laboratory
2200 N. Squirrel Rd.
Rochester, Michigan 48309

Sijin Wu
Mingli Dong
Beijing Information Science and Technology University
School of Instrument Science and Opto-Electronic Engineering
12 E. Xiaoyin Rd., Qinghe of Haidan District
Beijing 100192, China

Lianxiang Yang
Oakland University
Department of Mechanical Engineering
Optical Laboratory
2200 N. Squirrel Rd.
Rochester, Michigan 48309
E-mail: yang2@oakland.edu

Abstract. Digital shearography has demonstrated great potential in direct strain measurement and, thus, has become an industrial tool for non-destructive testing (NDT), especially for NDT of delaminations and detection of impact damage in composite materials such as carbon fiber reinforced plastics and honeycomb structures. The increasing demand for high measurement sensitivity has led to the need for real-time monitoring of a digital shearographic phase map. Phase maps can be generated by applying a temporal, or spatial, phase shift technique. The temporal phase shift technique is simpler and more reliable for industry applications and, thus, has widely been utilized in practical shearographic inspection systems. This paper presents a review of the temporal phase shift digital shearography method with different algorithms and the possibility for real-time monitoring of phase maps for NDT. Quantitative and real-time monitoring of full-field strain information, using different algorithms, is presented. The potentials and limitations for each algorithm are discussed and demonstrated through examples of shearographic testing. [DOI: 10.1117/1.OE.52.10.101902]

Subject terms: digital shearography; nondestructive testing; real time; phase map; temporal phase stepping.

Paper 121756SS received Nov. 29, 2012; revised manuscript received Feb. 13, 2013; accepted for publication Feb. 25, 2013; published online Apr. 8, 2013.

1 Introduction

Various full-field optical techniques such as digital shearography, digital holography, electronic speckle pattern interferometry (ESPI), thermography, and digital image correlation have been applied in recent years for full-field nondestructive testing (NDT).[1–6] Of these techniques, digital shearography has demonstrated many advantages for real-world applications.[7–11] Unlike other techniques, digital shearography uses a special shearing device to directly measure a displacement gradient rather than the displacement itself. This significant feature is particularly important for field NDT applications. Displacement gradients contain strain information and defects in materials generate strain concentration. As a result, digital shearography displays defects more directly. Rigid body motion also does not produce a displacement derivative. The relative insensitivity of digital shearography to environmental noises makes it better suited for field applications. Currently, digital shearography has become an industrial tool for NDT, especially, for NDT of delaminations in composite materials and honeycomb structures.[12–17]

There are two modes for displaying the testing results obtained from shearographic NDT which include the intensity fringe pattern and the phase map. The intensity fringe patterns are obtained by subtraction and squaring operations or taking an absolute value. Even though an intensity fringe pattern can be observed in real time, its measuring sensitivity and resolution is not as high as the phase map.[18] The intensity fringe pattern's smallest measurable phase value is 2π, and phase can only be measured at locations of fringe orders. It is true that a smaller phase value can be measured in the intensity fringe pattern by interpolation, and it should be good for quantitative measurement of deformation and strain such as in ESPI. However, it requires intensive computation and usually needs an off-line operation and, thus, the on-line and real-time measurement becomes impossible.

Furthermore, the interpolation enables the measurement of smaller phase values; however, it is unable to increase the spatial resolution. By comparison, the phase map mode can measure phase values much smaller than 2π with much high spatial resolution, usually to a resolution of $2\pi/30$ to $2\pi/50$, depending on such factors as speckle noise (due to the setup built) and software developed for the system.[19,20] In addition, the phase can be measured at the location of each pixel. Obviously, the phase map mode has much higher measuring sensitivity and resolution than the intensity fringe pattern mode for phase measurement. Therefore, it has a much higher sensitivity for measuring the displacement gradients because the phase is directly related to the displacement gradient in shearography. The increasing demand for on-line NDT by digital shearography has led to the need for a real-time monitoring of phase maps. Real-time monitoring can provide effective procedures allowing interaction of the operator such as applying proper load levels when inspecting unknown configurations. Furthermore, the operator can observe the evolution of defect-related phase changes which leads to higher reliability. A phase map can be generated by applying the temporal, or spatial phase, shift technique. It is generally considered that the temporal phase shift technique is better suited for static measurement while the spatial phase shift technique is suited more for dynamic measurement and has enormous potential for real-time display of the phase map.[21–24] Theoretically, this statement is true if a shearographic system is used under a laboratory condition. Practically, however, the spatial phase shift technique has not been accepted by commercialized shearographic NDT tools in field applications[15–17] because of its relative complexity in optics and a high requirement for precise adjustment of the optical setup. In the spatial phase shift shearography, carrier fringes are usually required. Carrier fringes can be generated by a Mach–Zehnder based interferometer by introducing an additional reference beam or by utilizing a multiple-aperture mask diffraction.[25–27] All of these techniques require precise adjustment of the reference mirror and beam or a specially designed multiple-aperture mask structure. If they are disarranged during transportation or field application, a complicated and fine adjustment is needed which does not meet the requirements of a practical industrial testing system.

The temporal phase shift technique is simple and reliable for industry applications.[28] Therefore, it has been widely utilized in practical shearographic inspection systems. The technique, however, needs to record three or more images, which makes real-time display of the phase maps difficult or impossible. In the last decade, different research groups have reported their attempts for measuring a phase distribution using only one speckle interference pattern acquired under dynamic conditions, such as $N+1$ ($N=3$, 4, and 5) clustering methods, $N+1$ least squares methods, and $N+1$ temporal phase shifting methods (also called as filtered secondary speckle interferograms methods).[1,2,8,29–31] The clustering algorithm is able to determine a phase change using only one loaded image; however, to determine the phase change on each single point, it needs the information from its multiple adjacent points, which requires high intensive computation. The algorithm is good for postprocessing instead of on-line and real-time test. Likewise, the least squares method also requires high intensive computation.

This paper will present a review of simple $N+1$ temporal phase shift methods for real-time display of phase map in shearography. A comparison of the display speed and phase map quality among $N+N$ ($N=3$, 4, and 5), $N+2$, and $N+1$ have been made. Quantitative and real-time monitorings of full-field strain information, using different algorithms, are presented. Each algorithm's potentials and limitations are discussed and demonstrated through examples of shearographic testing. For simplification, $3+3$, $3+2$, and $3+1$ algorithms has been selected for studying in details. The results obtained are also suited for $4+4$, $4+2$, $4+1$ and $5+5$, $5+2$, and $5+1$ algorithms.

2 Brief Review of Fundamental of Digital Shearography

Figure 1 shows a typical setup of digital shearography, which uses a modified Michelson interferometer as the shearing device. Tilting mirror 1 of the Michelson interferometer by a very small angle, the reflected laser rays from two points, P_1 and P_2, with a separation δx on the object surface, are brought into one point P on the image plane where the laser rays interfere with each other and a speckle interferogram is generated. The amount and the orientation of δx are called the shearing amount and the shearing direction, respectively. The intensity I of the resulting speckle interferogram of the unloaded object is given by[32]

$$I = a + b\cos\phi, \tag{1}$$

where a is the background of the interferogram, b is the modulation of the interference term, and ϕ is the phase difference between rays from points P_1 and P_2. The intensity of the resulting speckle interferogram is recorded by a charge-coupled device (CCD) camera and downloaded to a frame

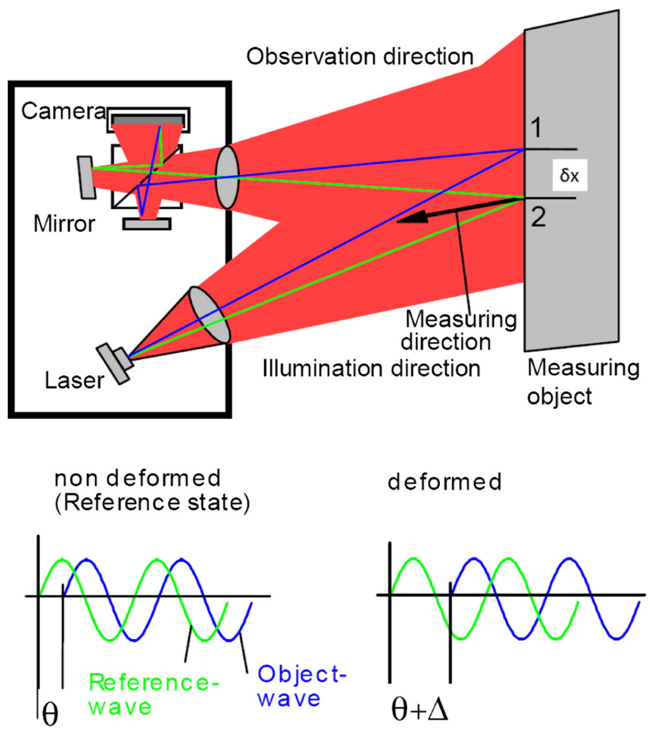

Fig. 1 Fundamental of digital shearography.

grabbing circuit board where the analog signals from the CCD array are digitized.

When the object is loaded, an optical path change occurs due to the deformation of the object's surface. The optical path change induces a relative phase change between rays from two points P_1 and P_2. Thus, the intensity distribution of the speckle interferogram is slightly altered; this is mathematically represented by

$$I' = a + b\cos(\phi + \Delta), \tag{2}$$

where I' is the intensity distribution after deformation and Δ is the relative phase change due to the relative displacement between the two points P_1 and P_2 in measuring direction.

2.1 *Display of Shearographic Test Result Using Intensity Fringe Pattern*

Subtraction between I' and I and displaying the absolute value of the subtraction data I_s (intensity value is always positive) results in a visible fringe pattern with the following representation:

$$|I_s| = |I' - I| = b|\cos(\phi + \Delta) - \cos\phi|. \tag{3}$$

At the locations where $\Delta = 2n\pi$, n is the fringe order which is equal to $0, 1, 2, 3, \ldots, I_s$ becomes zero, resulting in the formation of dark fringes. This is known as displaying mode through the intensity fringe pattern. If the intensity of the unloaded image I (reference image) is continuously subtracted from the intensity of loaded live image I' (loaded image), the visible fringe pattern can be observed in real time.

If the angle between the illumination direction of the laser and the observation direction of the camera is equal or close to zero, the relative phase change Δ is related to an out-of-plane displacement gradient ∂_w/∂_x (if the shearing direction is oriented in the x-direction) or ∂_w/∂_y (if the shearing direction is in the y-direction) and the relationships are given by[33,34]

$$\begin{aligned}\frac{\partial w}{\partial x} &= \frac{\lambda}{4\pi\delta x}\Delta \quad (\text{shearing in } x\text{-direction})\\ \frac{\partial w}{\partial y} &= \frac{\lambda}{4\pi\delta y}\Delta \quad (\text{shearing in } y\text{-direction}).\end{aligned} \tag{4}$$

In the intensity fringe pattern, the smallest measureable relative phase change Δ is 2π (if only one fringe is visible). Therefore, the minimum measurable displacement gradient is $\lambda/(2\pi\delta x)$ or $\lambda/(2\pi\delta y)$. In order to increase the measurement sensitivity for the displacement gradient, the sensitivity for measuring the relative phase change Δ has to be enhanced. The phase shift techniques have been applied for this purpose, which will be discussed in the following sections.

2.2 *Display of Shearographic Test Result Using Phase Map*

A phase ϕ of the speckle interferogram, as shown in Eq. (1), cannot be directly recorded by a CCD camera, but can be determined indirectly through three or more digitized intensity images using the phase shift technique.[35] The piezoelectric transducer (PZT) mirror, as shown in Fig. 1, is used for this purpose. As we know, there are three unknowns in a recorded intensity image [cf. Eq. (1)]. They are a background a, a modulation amplitude b, and the phase term ϕ. To determine the phase term ϕ, three or more images, with three equations, as shown in Eq. (5), are required:

$$\begin{aligned}I_1 &= a + b\cos(\phi)\\ I_2 &= a + b\cos(\phi + 120°)\\ I_3 &= a + b\cos(\phi + 240°).\end{aligned} \tag{5}$$

The 120 deg and 240 deg phase shifts can be obtained by moving the PZT mirror a distance of $\lambda/6$ between two adjacent images. Here, λ refers to the wavelength of the laser. The phase distribution ϕ can be determined from the above three digitized intensity values as follows:

$$\phi = \arctan\frac{\sqrt{3}(I_3 - I_2)}{2I_1 - I_2 - I_3}. \tag{6}$$

After the object is loaded, the interference phase ϕ changes the value to ϕ', which is equal to $\phi + \Delta$ [cf. Fig. 1 and Eq. (2)]. In the same way, ϕ' can be calculated by recording three additional images under the loading condition. A digital subtraction of ϕ from ϕ', as described in Eq. (7), generates a quantitative distribution of the relative phase change Δ, which is called a shearographic phase map.

$$\begin{aligned}\Delta &= \phi' - \phi\\ &= \arctan\frac{\sqrt{3}(I_3' - I_2')}{2I_1' - I_2' - I_3'} - \arctan\frac{\sqrt{3}(I_3 - I_2)}{2I_1 - I_2 - I_3}\\ &\quad (\text{add } 2\pi \text{ if } \Delta < 0),\end{aligned} \tag{7}$$

where I_1', I_2', and I_3' are the intensity of the three images after loading. Because the phase map is a fringe pattern with modulus 2π, a value of 2π should be added if the calculated Δ value is smaller than zero.[36]

The time required for recording three intensity images and for shifting the PZT mirror three times ranges from 400 to 500 ms, depending on the camera's frame rate and software program developed. For a camera with 15 frames per second (fps), the required time for capturing three images is 200 ms. A PZT can shift the mirror very fast (within a microsecond), but needs time to wait for the mirror to stabilize before the camera takes the next image. Usually, a 100 ms waiting time is adopted for each shift. Under these conditions, the total required time for data acquisition is about 500 ms. If the phase distribution under unloaded condition (reference phase) can be calculated before loading, the display rate of Eq. (7) mainly depends on the speed of the acquisition of data for the loaded object, which is about 500 ms. Accordingly, the displaying rate, for phase map by using the $3 + 3$ algorithm, can reach no more than two images per second. Thus, it is impossible for real-time observation.

2.3 *Comparison of Intensity Fringe Pattern and Phase Map Mode*

Figure 2 shows shearographic measurement results displayed using the intensity fringe pattern mode [Fig. 2(a)] and the phase map mode [Fig. 2(b)]. Even though an intensity fringe pattern can be observed in real time, it is only qualitative.

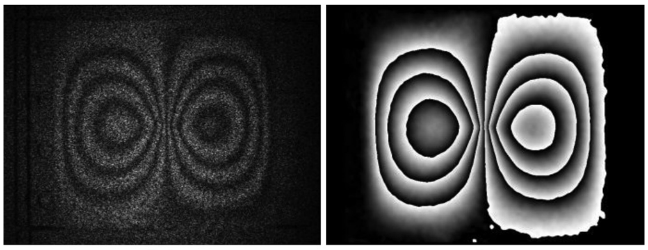

(a) (b)

Fig. 2 Two modes for displaying shearographic results: (a) intensity fringe pattern and (b) phase map; the sample is a fully clamped square plate with a load applied at the center of the plate from back side.

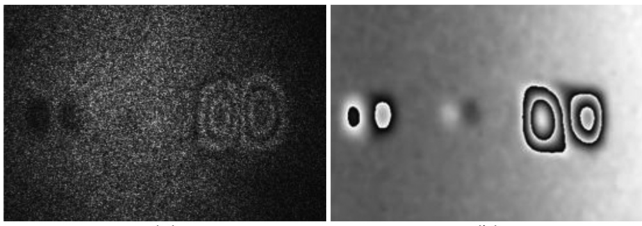

(a) (b)

Fig. 3 Intensity fringe pattern versus phase map of shearography for NDT of a composite plate with same vacuum loading. (a) The smallest delamination in the middle was not visible in the intensity mode. (b) All of the three delaminations were clearly identified in the phase map.

In the intensity fringe pattern, phases can be measured only at the locations of fringe orders and the smallest measurable phase value is 2π. By comparison, for the phase map mode, phase can be measured, quantitatively, at each pixel location, resulting in much higher spatial resolution. Theoretically, a relative phase change Δ can be measured at a very small value based on Eq. (7). Practically, however, it cannot be infinitely small due to speckle noise and spatial resolution of the digital camera. Usually, it can reach to a resolution of about $2\pi/30$. As a result, the phase map has a greater potential for measuring small defects.

Figure 3 shows a shearography measurement for a composite plate with three delaminations. The third and smallest delamination was not visible in the intensity fringe pattern, whereas all of the three delaminations were clearly identified in the phase map. Both tests utilized the same vacuum load.

Phase shift digital shearography has become an industry tool for NDT due to its quantitative and direct measurement of strain information with high measurement sensitivity. The increasing demand for inspection speed with different loading methods, such as dynamic loading, has led to the need for a real-time monitoring of phase maps of digital shearography. In the following section, we will discuss the possibility for real-time monitoring of phase maps of shearography using the temporal phase shift technique.

3 Real-Time Monitoring of Phase Map of Digital Shearography

If the phase of the unloaded object ϕ can be calculated before the start of measurement, then the display rate of relative phase change Δ $(=\phi' - \phi)$, i.e., the phase map, will depend mainly on the time of data acquisition for determining the phase of the loaded object ϕ'. According to Eq. (1), a, b, and the phase ϕ are the three unknowns in a digitized intensity equation. After the object is loaded, a and b remain constant, while the phase ϕ becomes ϕ'. The two intensity equations, taken before and after loading, consist of a total of four unknowns which are a, b, phase ϕ before loading, and phase ϕ' after loading. Four or more intensity equations (images) are required to determine these unknowns. The $3+3$ algorithm uses six equations to determine the phase map. It is too slow because the displaying rate is limited to 2 fps. To increase the display rate, the number of images taken should be reduced. Two other methods can be utilized such as $3+2$ (5 images) and $3+1$ (4 images) methods.

3.1 $3+2$ *Method*

In the $3+2$ method, three images (three equations) are recorded before loading and two images (two equations) are recorded after loading as shown in Eq. (8):

$$\begin{array}{ll} I_1 = a + b\cos(\phi) & \\ I_2 = a + b\cos(\phi + 120°) \quad \text{and} & I_1' = a + b\cos(\phi+\Delta) \\ I_3 = a + b\cos(\phi + 240°) & I_2' = a + b\cos(\phi+\Delta+120°). \\ (\text{before loading}) & (\text{after loading}) \end{array} \tag{8}$$

From the images taken before loading, the phase ϕ can be determined using Eq. (6). In addition, the parameter a can also be solved:

$$a = \frac{I_1 + I_2 + I_3}{3}. \tag{9}$$

Based on the two equations taken after loading and Eq. (9), the phase of loaded object ϕ', which is equal to $(\phi + \Delta)$, is solved:

$$\begin{aligned} \phi + \Delta &= \arctan\frac{3a - 2I_2' - I_1'}{\sqrt{3}(I_1' - a)} \\ &= \arctan\frac{\sqrt{3}(I_1 + I_2 + I_3 - 2I_2' - I_1')}{3I_1' - (I_1 + I_2 + I_3)}. \end{aligned} \tag{10}$$

A subtraction of ϕ from ϕ' generates a phase difference Δ, or shearographic phase map:

$$\begin{aligned} \Delta &= \arctan\frac{\sqrt{3}(I_1 + I_2 + I_3 - 2I_2' - I_1')}{3I_1' - (I_1 + I_2 + I_3)} \\ &\quad - \arctan\frac{\sqrt{3}(I_3 - I_2)}{2I_1 - I_2 - I_3} \qquad (\text{add } 2\pi \times \text{if } \Delta < 0). \end{aligned} \tag{11}$$

One can also use 90 deg phase shift for the loaded images. In this case, the phase shift of 120 deg should be replaced by 90 deg, and the relative phase change Δ becomes

$$\begin{aligned} \Delta &= \arctan\frac{I_1 + I_2 + I_3 - 3I_2'}{3I_1' - (I_1 + I_2 + I_3)} - \arctan\frac{\sqrt{3}(I_3 - I_2)}{2I_1 - I_2 - I_3} \\ &\quad \times (\text{add } 2\pi \times \text{if } \Delta < 0). \end{aligned} \tag{12}$$

The $3+2$ method is based on an assumption that a and b, in Eq. (8), remain constant before and after a loading. In reality, a and b may not be identical due to decorrelation of some speckles which will result in more noises. This is the reason why the phase map of $3+3$ method has better quality than that of the $3+2$ method. In Sec. 3, we shall demonstrate the phase maps of the methods.

The time required for capturing two intensity images of loaded object and shifting the PZT mirror two times for a camera with a data acquisition speed of 15 fps is about 335 ms. With this time value required, the displaying rate of the phase map can reach a speed of about three images per second if everything is optimized. Though the displaying speed is increased, it is still not fast enough and, therefore, is still not suited for dynamic loading.

3.2 $3+1$ *Method*

In the $3+1$ method, three images (three equations) are recorded before loading and one image, with no phase shift, is recorded after loading, as shown in Eq. (13):

$$\begin{array}{ll} I_1 = a + b\cos(\phi) & \\ I_2 = a + b\cos(\phi + 120°) & \text{and} \quad I' = a + b\cos(\phi + \Delta) \\ I_3 = a + b\cos(\phi + 240°) & \\ \text{(before loading)} & \qquad \text{(after loading)} \end{array}. \tag{13}$$

The algorithm for calculating the relative phase change Δ, using the $3+1$ method, is somewhat complicated. Subtracting I' from I_1, I_2, and I_3, respectively, and taking the square of the three subtracted results generates the following three equations:

$$\begin{aligned} (I_1 - I')^2 &= 4b^2 \sin^2(\phi + \Delta/2)\sin^2(\Delta/2) \\ (I_2 - I')^2 &= 4b^2 \sin^2(\phi + \Delta/2 + \pi/3)\sin^2(\Delta/2 - \pi/3) \\ (I_3 - I')^2 &= 4b^2 \sin^2(\phi + \Delta/2 + 2\pi/3)\sin^2(\Delta/2 - 2\pi/3). \end{aligned} \tag{14}$$

Though $\Delta/2$ is a low-frequency component (induced by a loading), the phase ϕ (phase difference between two points P_1 and P_2, as seen in Fig. 1) is a high-frequency component due to the surface roughness. The terms $(\phi + \Delta/2)$, $(\phi + \Delta/2 + \pi/3)$, and $(\phi + \Delta/2 + 2\pi/3)$ are also high-frequency components. For the high-frequency term, a detector captures the average value of the term within each speckle.[35] With this assumption, we have the following result:

$$\begin{aligned} \left[\sin^2\left(\frac{\Delta}{2} + \theta\right)\right] &\approx \frac{1}{2n\pi}\int_0^{2n\pi} \sin^2\left(\frac{\Delta}{2} + \theta\right) d\left(\frac{\Delta}{2} + \theta\right) \\ &= \frac{1}{2}, \end{aligned} \tag{15}$$

where n is an integer number. The feasibility of equation is based on the assumption that the speckle size is smaller than the pixel size so that a pixel will cover several speckles. In our experiment, the pixel size of the CCD camera is about 17 μm and the speckle diameter is about 6 μm (depending on aperture size). In this case, one pixel will cover about nine speckles. Therefore, the phase range covered by one pixel is enough to meet the assumption. If a higher resolution camera, such as a five mega camera, will be used, the pixel size will be significantly reduced. Consequently, the average effect will be reduced and more noises will be introduced. However, on the other hand, the high-resolution camera significantly increases the spatial resolution, which is more important for inspecting smaller defects in objects, because the high-frequency noises can be suppressed by enlarging the lens aperture or applying a low-pass filter. With the result shown in Eq. (15), Eq. (14) can be simplified as follows:

$$\begin{aligned} (I_1 - I')^2 &\approx 2b^2 \sin^2(\Delta/2) = b^2[1 - \cos(\Delta)] \\ (I_2 - I')^2 &\approx 2b^2 \sin^2(\Delta/2 - \pi/3) = b^2[1 - \cos(\Delta - 2\pi/3)] \\ (I_3 - I')^2 &\approx 2b^2 \sin^2(\Delta/2 - 2\pi/3) = b^2[1 - \cos(\Delta - 4\pi/3)]. \end{aligned} \tag{16}$$

The distribution of the relative phase change Δ, i.e., the shearographic phase map, can then be determined by

$$\Delta = \arctan\frac{\sqrt{3}[(I_3 - I')^2 - (I_2 - I')^2]}{2(I_1 - I')^2 - (I_2 - I')^2 - (I_3 - I')^2}. \tag{17}$$

For a camera with 15 fps, the display rate can reach higher than 10 images per second, allowing the phase map to be observed in real time. Furthermore, the technique can be applied for dynamic analysis, if combined with a high-speed camera.

4 Discussion, Comparison, and Demonstrations

Figure 4 shows a comparison of three shearographic phase maps created by the $3+1$, $3+2$, and $3+3$ methods, respectively (from left to right). The three phase maps were taken from the same object using the same loading and smoothed twice by the same window size (5×5 window).

From the point of view of the speed for displaying the phase map, the display rate for the $3+1$ method can reach 10 images per second or higher depending on the camera speed. The method enables real-time observation of phase map. It is well suited for shearographic NDT while a continued loading, such as a thermal loading, an internal press, or a vacuum loading, is needed to make all flaws visible. Figure 5 shows inspection results for the composite plate, shown in Fig. 3, using the $3+1$ real-time phase map observation method and an increasing vacuum load. All three delaminations were clearly identified when the vacuum loading increases to -8 kPa. This function will make shearographic testing more convenient for real-world applications.

With respect to the image quality, Fig. 4 shows that the $3+3$ method has the best quality, the quality of $3+2$ method is still quite good, and the $3+1$ method has more noise than the other two. Though the $3+1$ method has more noise, it is still an acceptable level for NDT. The camera used in the investigation, shown in Fig. 4, has 640×480 pixels. Should a camera with higher spatial resolution be utilized, the quality of the phase map will increase. Despite good quality in the $3+3$ and $3+2$ methods, the displaying speed for phase map is approximately two images per second for the $3+3$ method and three images per second for the $3+2$ method. Obviously, the applications are mainly limited to static or quasi-static loading.

A further significant feature of the $3+1$ method is its ability for dynamic applications. The $3+1$ method has great potential, in combination with a high-speed camera, to generate phase maps for digital shearography in dynamic measurement because only a single image is needed under

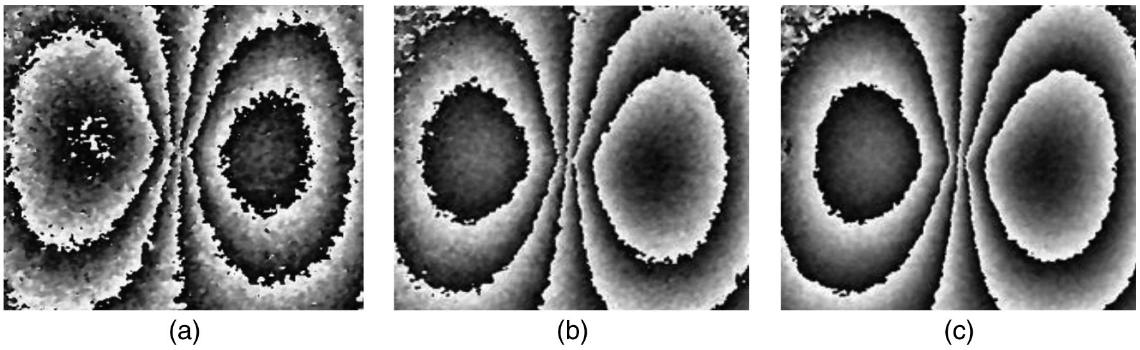

Fig. 4 A comparison of phase maps created by (a) $3 + 1$, (b) $3 + 2$, and (c) $3 + 3$ methods.

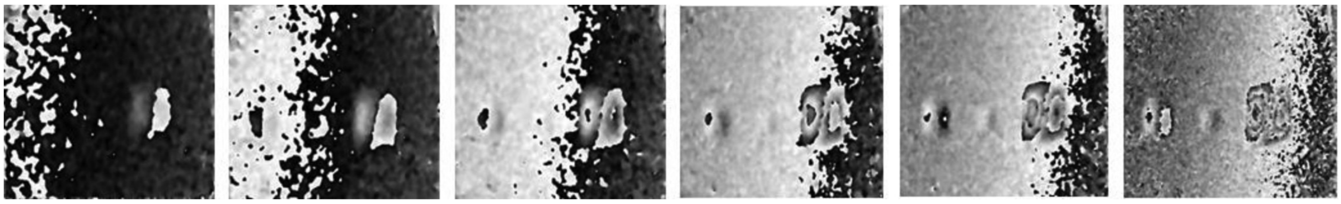

Fig. 5 Shearographic NDT by real-time observation of phase map by using $3 + 1$ method, loading increasing from left to right and all three delaminations were clearly detected while the vacuum increases to −8 kPa (the most right image).

a loaded condition. Figure 6 shows our attempt using the $3 + 1$ method and a high-speed digital shearographic system for NDT. The sample is an aerospace honeycomb plate with a delamination. First, the three initial images were taken statically before loading. Based on Eq. (5), a phase shift of 120 deg was introduced between two adjacent images. Then, the sample was heated, by a normal heat gun, for about 20 s. After waiting for about 5 s, a series of images were captured by a high-speed camera as the temperature drops. Because the loading is not really dynamic and the laser power is not high enough, a rate of only 100 fps was taken. The phase maps shown in Fig. 6 were picked every 30 images, one every 300 ms, and calculated by Eq. (17) together with the first recorded three images. The delamination area can be obviously located in the phase maps. The temperature in these images was dropping from left to right and from top to bottom. Because the reference is an unheated object, the phase map at the top left has the most fringes and the phase map at the bottom right has the fewest fringes. Though this trial was taken at a rate of 100 fps, the result has demonstrated that the $3 + 1$ temporal phase shift technique is capable of dynamic measurement and has great

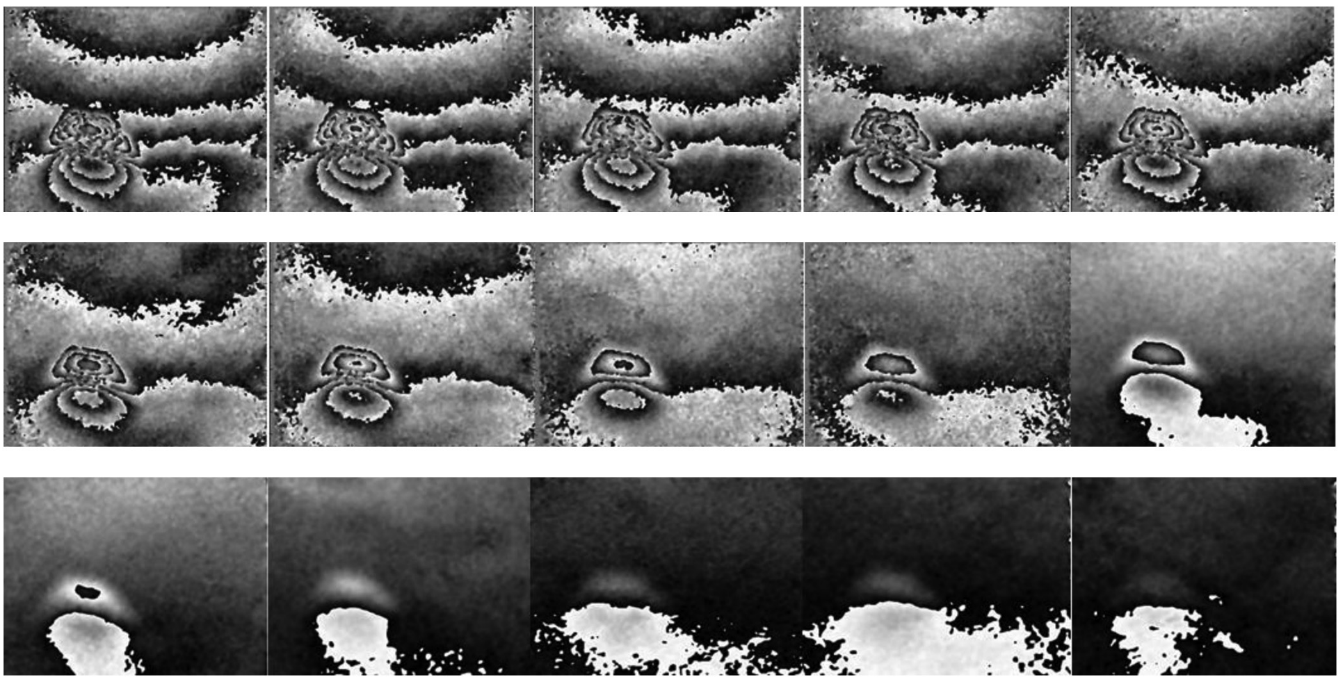

Fig. 6 NDT with high-speed digital shearographic system for inspection of a honeycomb plate with a delamination while temperature dropping (from top left to bottom right).

potential for phase shift shearography for NDT under dynamic loading such as with harmonic excitation or with impact testing.

Despite many advantages, the $3 + 1$ method has some limitations. Three reference images must be taken while object is unloaded. Refreshing these reference images during measurement is impossible, which limits the load magnitude that can be applied. If the reference images need to be refreshed, the object to be tested must be under a stable condition. The background a and modulation of the interference term b in the intensity equation must also be exactly identical while taking intensity measurements of the unloaded and loaded object. This means that the background a and modulation of the interference term b of the laser used should be stable with time. If a diode laser will be utilized, it must be in possession of current and temperature stabilization functions.

Due to the limited length of the content, this paper only reviews and compares $3 + 3$, $3 + 2$, and $3 + 1$ algorithms. It should be emphasized that all potentials and limitations discussed and presented in this paper are suited for $4 + 4$, $4 + 2$, $4 + 1$ and $5 + 5$, $5 + 2$, $5 + 5$ due to similar fundaments as well. In summary, $N + N$ ($N = 3$, 4, and 5) methods have the best quality for phase map; however, it is suited for on-line testing only with a static loading. For a camera with a data acquisition speed of 15 fps, the displaying speed for phase map is approximately 2, 1.5, and 1.2 images per second for the $3 + 3$, $4 + 4$, and $5 + 5$ methods, respectively. $N + 2$ methods still have a good quality in phase maps as they can reach approximately three images per second for all of the $3 + 2$, $4 + 2$, and $5 + 2$ methods and are suited for on-line shearographic NDT with a quasi-static loading. Finally, $N + 1$ methods have the fastest displaying speed for phase maps, which can reach 10 images per second or higher, depending on the camera speed. The $N + 1$ methods enable real-time monitoring of phase map and make shearographic test more convenient for real-world applications. Furthermore, $N + 1$ methods are capable of dynamic applications. The phase maps in $N + 1$ methods have a little more noise but are still in an acceptable level for the applications of NDT. Regarding the N number, there is no big difference in using 3, 4, or 5 method in shearographic NDT if the main purpose is to just inspect defects.

5 Conclusion

This paper has presented a review of the temporal phase shift digital shearography using $3 + 3$, $3 + 2$, and $3 + 1$ algorithms and the possibility for real-time monitoring of the phase maps for NDT. Displaying phase map of digital shearography enhances the measurement sensitivity which offers the possibility for NDT of smaller defects in different materials. A real-time monitoring of the phase maps makes the measurement more convenient and effective. Theoretical analysis, and experimental, tests have demonstrated that the $3 + 1$ method is capable of real-time monitoring of phase maps with a simple concept and a simple optical setup. Experimental investigations also indicate that the $3 + 1$ method has great potential for high speed, digital shearographic, NDT with dynamic loading. Likewise, the $4 + 1$ or $5 + 1$ method has the same features as described above. For better understanding of the usefulness, the limitations of different algorithms have also been presented and discussed. This paper has provided useful information for researchers who are planning to use simple temporal phase shift technique for real-time monitoring of phase map of digital shearography and for the NDT with dynamic loading.

Acknowledgments

The authors would also like to express their sincere thanks to Mr. Bernard Sia, PhD candidate of the Optical Laboratory at Oakland University, who carefully and thoroughly read the manuscript and provided valuable criticisms. The work is supported by the National Natural Science Foundation of China under grants 51275054 and 51075116, and the International Science and Technology Cooperation Plan of Anhui Province (No. 12030603012).

References

1. D. Francis, R. P. Tatam, and R. M. Groves, "Shearography technology and applications: a review," *Meas. Sci. Technol.* **20**(10), 102001 (2010).
2. W. Steinchen and L. X. Yang, *Digital Shearography: Theory and Application of Digital Speckle Pattern Shearing Interferometry*," SPIE Press, Bellingham, WA (2003).
3. Y. Y. Hung, H. M. Shang, and L. X. Yang, "Unified approach for holography and shearography in surface deformation measurement and nondestructive testing," *Opt. Eng.* **42**(5), 1197–1207 (2003).
4. L. X. Yang and A. Ettemeyer, "Strain measurement by 3D-electronic speckle pattern interferometry: potentials, limitation and applications," *Opt. Eng.* **42**(5), 1257–1266 (2003).
5. X. Chen et al., "High temperature displacement and strain measurement using a monochromatic light illuminated stereo digital image correlation system," *Meas. Sci. Technol.* **23**(12), 125603 (2012).
6. Y. Y. Hung et al., "Review and comparison of shearography and active thermography for nondestructive evaluation," *Mater. Sci. Eng. R* **64**(5), 73–112 (2009).
7. L. X. Yang, "Recent developments in digital shearography for nondestructive testing," *Mater. Eval.* **64**(7), 704–709 (2006).
8. Y. H. Huang et al., "NDT&E using shearography with impulsive thermal stressing and clustering phase extraction," *Opt. Laser Eng.* **47**(7), 774–781 (2009).
9. C. J. Tay and Y. Fu, "Determination of curvature and twist by digital shearography and wavelet transforms," *Opt. Lett.* **30**(21), 2873–2875 (2005).
10. W. Steinchen et al., "Nondestructive testing of aerospace composite materials using digital shearography," *J. Aerosp. Eng.* **212**(1), 21–30 (1998).
11. T. W. Ng, "Shear measurement in digital speckle shearing interferometry using digital correlation," *Opt. Comm.* **115**(3), 241–244 (1995).
12. M. Kalms and W. Osten, "Mobile shearography system for the inspection of aircraft and automotive components," *Opt. Eng.* **42**(5), 1188–1196 (2003).
13. M. Schuth, F. Voessing, and L. X. Yang, "A shearographic endoscope for nondestructive test," *J. Holography Speckle* **1**(1), 46–52 (2004).
14. S. J. Wu, X. Y. He, and L. X. Yang, "Enlarging the angle of view in Michelson interferometer-based shearography by embedding a 4f system," *Appl. Opt.* **50**(21), 3789–3794 (2011).
15. Dantec Dynamics GmbH, "Shearography–Non Destructive Testing," http://www.dantecdynamics.com/Default.aspx?ID=665.
16. Laser Technology Inc., "Laser Shearography Technology," http://www.laserndt.com/technology/shearography.htm.
17. Steinbichler Inspiring Innovation, "Shearography NDT," http://www.steinbichler.com/products/surface-scanning/shearography-ndt.html.
18. J. R. Huang, H. D. Ford, and R. P. Tatam, "Phase-stepped speckle shearing interferometry by source wavelength modulation," *Opt. Lett.* **21**(18), 1421–1423 (1996).
19. D. C. Ghiglia and M. D. Pritt, *Two-Dimensional Phase Unwrapping: Theory, Algorithms, and Software*," Wiley, New York (1998).
20. L. X. Yang and T. Siebert, "Digital speckle interferometry in engineering," in *New Directions in Holography and Speckle*, H. J. Caulfield and C. Vikram, Eds., pp. 405–440, American Scientific Publishers, Stevenson Ranch, California (2008).
21. A. Fernández et al., "Measurement of transient out-of-plane displacement gradients in plates using double-pulsed subtraction TV shearography," *Opt. Eng.* **39**(8), 2106–2113 (2000).
22. J. M. Huntley, "Automated analysis of speckle interferograms," in *Digital Speckle Interferometry and Related Techniques*, P. K. Rastogi, Ed., pp. 59–83, Wiley, Chichester (2001).
23. A. Dávila, G. H. Kaufmann, and C. Pérez-López, "Transient deformation analysis by a carrier method of pulsed electronic speckle-shearing pattern interferometry," *Appl. Opt.* **37**(19), 4116–4122 (1998).

24. F. Santos, M. Vaz, and J. Monteiro, "A new set-up for pulsed digital shearography applied to defect detection in composite structures," *Opt. Laser Eng.* **42**(2), 131–140 (2004).
25. G. Pedrini, Y. L. Zou, and H. J. Tiziani, "Quantitative evaluation of digital shearing interferogram using the spatial carrier method," *Pure Appl. Opt.* **5**(3), 313–321 (1996).
26. X. Xie et al., "Simultaneous measurement of deformation and the first derivative with spatial phase-shift digital shearography," *Opt. Comm.* **286**(1), 277–281 (2013).
27. B. Bhaduri et al., "Use of spatial phase shifting technique in digital speckle pattern interferometry (DSPI) and digital shearography (DS)," *Opt. Exp.* **14**(24), 11598–11607 (2006).
28. L. X. Yang et al., "Digital shearography for nondestructive testing: potentials, limitations and applications," *J. Holography Speckle* **1**(2), 69–79 (2004).
29. K. Li and K. Qian, "Dynamic phase retrieval in temporal speckle pattern interferometry using least squares method and windowed Fourier filtering," *Opt. Exp.* **19**(19), 18058–18066 (2011).
30. C. C. Kao et al., "Phase-shifting algorithms for electronic speckle pattern interferometry," *Appl. Opt.* **41**(1), 46–54 (2002).
31. M. Hipp, W. Fliesser, and T. Nerger, "Temporal resolved phase stepped speckle interferometry of instationary plasma discharges," *Proc. SPIE* **3745**, 366–376 (1999).
32. J. A. Leendertz and J. N. Butters, "An image-shearing speckle-pattern interferometer for measuring bending moments," *J. Phys. E: Sci. Instrum.* **6**(11), 1107–1110 (1973).
33. R. Kästle, E. Hack, and U. Sennhauser, "Multiwavelength shearography for quantitative measurements of two-dimensional strain distributions," *Appl. Opt.* **38**(1), 96–100 (1999).
34. R. M. Groves, S. W. James, and R. P. Tatam, "Full surface strain measurement using shearography," *Proc. SPIE* **4448**, 142–152 (2001).
35. K. Creath, "Phase shifting speckle interferometry," *Appl. Opt.* **24**(18), 3053–3058 (1985).
36. S. Liu and L. X. Yang, "Regional phase unwrapping method based on fringe estimation and phase map segmentation," *Opt. Eng.* **46**(5), 051012 (2007).

Lianqing Zhu is a professor of the School of Instruments Science and Opto-Electronic Engineering at Beijing Information Science and Technology University in China. He has multidisciplinary research experiences including optical metrology, biomedical detection technology, and 3-D computer vision. He is the director of Beijing Engineering Research Center of Photoelectric Information and Instruments, a council member of Chinese Society for Measurement, and an executive member of the council and assistant secretary general at Mechanical Quantity Measurement Instrument Federation of China Instrument and Control Society.

Yonghong Wang received his PhD degree in precision mechanical engineering from Hefei University of Technology, China, in 2004. He was a postdoctoral fellow in the Optical Laboratory at Oakland University in Michigan from 2007 to 2008. He is currently a professor in the School of Instrument Science and Opto-Electronic Engineering, Hefei University of Technology. He has authored and co-authored over 30 scientific research papers and has owned four Chinese patents in the areas of optical techniques for whole-field and 3-D measurement. His current research interests are precision metrology, advanced optical measuring techniques, and image processing and their applications for the automotive, high-tech, and biomedical industries.

Nan Xu is a PhD candidate in the Optical Laboratory of Mechanical Engineering at Oakland University. He received BE in computer science from Northeastern University, Shenyang, China, in 2000 and ME in optical engineering from Beijing Jiaotong University, China, in 2008. His research interests include optical metrology, nondestructive testing with digital shearography experimental strain/stress analysis, nondestructive testing, 3-D computer vision, and software programming and development.

Sijin Wu received his PhD degree in optical engineering from Beijing Jiaotong University, China, in 2012. Prior to receiving his PhD degree, he was an exchanged PhD student in the Optical Laboratory at Oakland University for two years. He joined Beijing Information Science and Technology University in July 2012 as a faculty member. His research interests include optical metrology, such as digital holography and digital shearography, experimental strain/stress analysis, nondestructive testing, and 3-D computer vision.

Mingli Dong received her PhD in physical electronics from Beijing Institute of Technology, China. She is a professor in the School of Instruments Science and Opto-Electronic Engineering at Beijing Information Science and Technology University in China and the head of the Department of Measurement and Control Technology and Instruments. She has multidisciplinary research experiences including vision measuring technology, optical metrology, and biomedical detection technology.

Lianxiang Yang received his PhD in mechanical engineering from the University of Kassel, Germany, in 1997. He is the director of Optical Laboratory and a professor in the Department of Mechanical Engineering at Oakland University in USA. Prior to joining Oakland University in 2001, he was an R&D scientist at JDS-Uniphase, Canada, from 2000 to 2001, a senior engineer at Dantec-Ettemeyer AG (currently called Dantec-Dynamics GmbH), Germany, from 1998 to 2000, a research and senior research fellow at the University of Kassel, Germany, from 1991 to 1998, and a lecturer at Hefei University of Technology, China, from 1986 to 1991. He has multidisciplinary research experiences including optical metrology, experimental strain/stress analysis, nondestructive testing, and 3-D computer vision. He is a Fellow of SPIE, a Changjiang scholar of Hefei University of Technology, and an adjunct professor of Beijing Information Science and Technology University.